The effect of biochar filler on the hydration products and microstructure in Portland cement stabilized peat

Debora Berti[1], Giovanna Biscontin, Ph.D[2], and Jeffrey Lau, Ph.D.[3]

[1]PhD Student, Texas A&M University, Department of Oceanography, MS 3146, College Station, TX 77843 Email: debora-berti@tamu.edu

[2]University Lecturer, Department of Engineering, University of Cambridge, Trumpington Street, Cambridge CB2 1PZ, UK, Email: gb479@cam.ac.uk

[3] PhD Graduate, Department of Engineering, University of Cambridge, Trumpington Street, Cambridge CB2 1PZ, UK, Email:jeffreylauze@gmail.com

ABSTRACT

Laboratory tests demonstrated that biochar filler added to Portland cement stabilized peat results in an increase of unconfined compressive strength, comparable with that of a sand filler. Strength increase is significantly higher when biochar is ground to a size below 75 μm. This paper investigates the changes in mineralogy, texture and microstructure during the early hydration of cement mixed with peat and biochar filler to identify the mechanisms responsible for the strength increase. The results show that the biochar surface catalyzes nucleation of hydration products. Labile carbon in biochar promotes carbonation, with precipitation of calcite within its cells and on its surface, as well as formation of hemi and monocarboaluminate, two stable AFm phases. For the

larger fragments of biochar, the early hydration products do not reach the inner cells. Instead, the fine fragments tend to be fully covered leading to a more homogeneous spatial distribution of cement and voids.

INTRODUCTION

Peat soil is a type of soft soil with extremely high organic and water contents. It forms from the accumulation of undecomposed and partially decomposed organic matter, in a water saturated environment (up to 1000% water content) where scarcity of oxygen and reducing conditions favor preservation of organics. Peat soils are widespread in temperate and cold zones of the northern hemisphere and in the lowland areas of Southeast Asia (Osman 2018). One of the major issues with construction on peat soil is its high compressibility, causing structures to experience large undesirable differential settlement. Chemical stabilization by using artificial binders has been largely successful in treating soft soil. When chemical binders, such as cement, are added to soil in the presence of water, cementitious and pozzolanic reactions occur to form cementitious gels which increase the strength of the soil matrix. Organic matter in peat inhibits or slows down these reactions (Tremblay, et al. 2002). Therefore, a large quantity of binder is required before a significant strength gain is observed (Janz and Johansson 2002). Typically, sand is added to the stabilization mix as an inert filler, to reduce the amount of binder required. Urbanization driven, rapid growth of global cement production has escalated the extent of sand mining to surpass natural renewal rates (Larson 2018) thus

making the search for alternative fillers a critical need.

Lau et al. (2019) propose biochar as a sustainable, highly available alternative to sand. As biochar can be produced from local biomass, usually abundant in regions with peat soil, it can supply filler for treatments of large volumes of soil, such as in transportation infrastructure application (e.g. road sub-base). Biochar is the carbon-rich product of the pyrolysis of biomass. It stores Carbon in a recalcitrant form, significantly slowing down its re-emission into the atmosphere as CO_2 (Woolf, et al. 2010). According to Lehman and Joseph (2015), a sustainable conversion of 1% annual plant uptake into biochar can reduce atmospheric CO_2 by 10% of current anthropogenic emissions.

Biochar most common application is in soil amendment because its water and nutrient retention capacity lead to a significant improvement in crop productivity (Woolf, et al. 2010, Bruun, et al. 2014, Lehmann and Joseph 2015). Additionally, biochar has been investigated for removal of pollutants (Park, et al. 2011, Tan, et al. 2015), as a catalyst, in fuel cells and other environmental applications (Qian, et al. 2015). In recent years, the feasibility of using biochar in construction material has been explored (Gupta and Kua 2017, Gupta, et al. 2018, Dixit, et al. 2019, Wang, et al. 2020). A few studies showed that addition of 1-2% hardwood-derived biochar to Ordinary Portland Cement (OPC) accelerates hydration, with a corresponding increase of unconfined compressive strength (UCS), at seven days (Gupta, et al. 2018, Dixit, et al. 2019, Wang, et al. 2020). Gupta et al. (2018) proposed that slowly released water by the biochar promotes formation of

hydration products. Dixit et al. (2019) noted a positive effect of fine-size biochar (<150 μm) filler on the early hydration rate in ultra-high performance concrete. The correlation between fine size and faster hydration has been shown for sand fillers too and has been attributed to a better filling of the space by fine particles. Wang et al. (2020) tested the effect of CO_2 curing of OPC with biochar filler (1%). They observed carbonation of portlandite and faster rate of hydration, with an overall positive effect on strength.

Lau et al. (2019) tested the effect on compressive strength of a biochar filler added to high-water-content peat OPC mixtures, compared to a sand filler. Results showed comparable performance between the two. Most importantly, UCS of mixtures made with biochar ground to a fine particle size (< 75 um) decisively surpassed that of mixtures made with equivalent size and weight of sand. This unexpected, measurable difference in UCS, clearly related to the presence of fine-grained biochar, raises the question of whether biochar influences the type and extent of the hydration reactions or causes microstructural and textural changes that favor strength development. This paper addresses the mechanisms by which biochar affects strength development.

The mineralogy, texture and microstructure of mixtures of 1000% water content peat, OPC and different particle-size biochar filler were characterized by Scanning Electron Microscopy (SEM), combined with Energy-Dispersive X-ray Spectroscopy (EDS), and Powder X-Ray Diffraction (XRD). The same samples that were used for UCS testing by Lau et al. (2019) were investigated after seven days of curing. The peat-OPC-biochar

mixture prepared with biochar size below 75 μm, was further tested at 28 and 120 days by XRD to investigate potential changes in hydration products and the progression of the hydration reaction. The results of this study provide the groundwork for the long-term prediction of the cement stabilized soil strength and of the effects of large-scale use.

MATERIALS AND METHODS

Preparation of Peat, OPC, Biochar Mixtures

Five mixtures of peat-biochar-cement, differing only in the grain size of biochar, and a control sample consisting of peat and cement were investigated in this study. The peat was reconstituted to a water content of 1000%. This value falls into the middle of the natural water content range of peat soils, according to a review by Huat (2004). The source and preparation of peat and cement is described in detail in the paper by Lau et al. (2019) and is summarized here. Peat, sourced from Irish bogs owned by the Bord na Mona company, was obtained from a local garden center. It is a brown peat, with moderately strong humification, corresponding to the H6 class of the von Post scale (Hartlén and Wolski 1996). The peat has low fiber content, zero tensile strength, and a pH of 3.6. The peat purchased for this study had been previously dried thus its natural water content is not known. Bags of peat were mixed thoroughly in bulk to ensure homogeneity and sieved to remove debris larger than 5 mm. Tap water was added to the peat and mixed in a paint paddle mixer until a water content of 1000% was reached. The reconstituted peat had a bulk density of 976 kg/m^3. The biochar, produced by BioRegional, was derived

100 from sustainably sourced timber wood chips pyrolyzed at 450°C for 48 hours. It was
101 graded into five different particle size ranges, named A to E, from the coarsest (5-2 mm
102 range) to the finest (< 75 μm), to yield five differently graded mixtures, as shown in Table
103 1. Biochar was dried in the oven at 50°C for 24 hours to remove moisture while preserving
104 the integrity of its micropores, prior to mixing with the peat. The pH of biochar, measured
105 after dilution with distilled water, was 8.1.

106 Mixtures were prepared starting with the reconstituted peat, by adding 20% by weight
107 of biochar and 20% by weight of OPC. Biochar and OPC were added sequentially, each
108 addition followed by mixing for 5 minutes at medium speed. The mixture was then
109 spooned into lightly greased, 70 mm PVC split molds in five layers. After each of the 5
110 layers, the mixture was pushed down gently using a fork and tamped 10 times, with a
111 30 mm diameter cylindrical aluminum rod. The samples were left to cure in a large tank
112 filled with water halfway up the sides of the molds, allowing water to flow in. All
113 specimens were cured for 7 and 28 days; a few specimens cured for up to 120 days.

114 Unconfined compressive strength tests were conducted according to ASTM D2166
115 (ASTM, 2013). Triplicate specimens were run after 7 and 28 days for all samples.

116 **Analytical Methods**

117 Samples were analyzed by Scanning Electron Microscopy (SEM), with a
118 Thermofisher/FEI Quanta 600, equipped with a dedicated solid state backscatter detector
119 and a Bruker silicon drift detector (SDD) for Energy Dispersive X-ray Spectroscopy (EDS)

120 of elements with atomic number higher than B. After 7 days of curing, a set of samples
121 was air dried and coated with Pt/Pd, to limit charging, while another set was dehydrated
122 by methanol exchange, embedded in Spurr epoxy resin (modified according to Ellis,
123 2006), polished down to 0.5 μm, and coated with Pt/Pd. Air dried samples were analyzed
124 in secondary mode (SE) at 10 keV to observe the morphology of the grains and
125 components of the mixture. In secondary mode, image contrast is mainly a function of
126 topography. Polished samples were instead analyzed in backscatter mode (BSE) which
127 gives micrographs where gray contrast is a function of average atomic number of the
128 material, with higher contrast corresponding to higher atomic number. EDS spectra were
129 collected by point analysis from the polished blocks, and a few from particles in the air-
130 dried samples. An operating voltage of 20 keV was used for EDS microanalysis.

131 Mineral composition of samples cured for 7 days was analyzed by powder X-ray
132 diffraction (XRD), with a Siemens D500 diffractometer, using Cu−kα radiation and
133 operated at 40 kV and 40 mA. Samples were scanned between 3 and 65°2θ, at steps of
134 0.05°2θ and 4 sec/step counting time. Additional XRD were acquired from samples A and
135 E after 28 days of curing and on sample E after 120 days, by a Bruker D8 Advance
136 diffractometer, using Cu − kα radiation, and operated at 40 kV and 40 mA , using the
137 same acquisition settings.

138 Phase quantification for the crystalline fraction was computed by Rietveld analysis
139 using the program BGMN (Taut, Kleeberg and Bergmann 1998), accessed through the

Profex graphical interface (Döbelin and Kleeberg 2015). The program BGMN-Profex models mineral peaks in the XRD pattern by deconvolution of the wavelength distribution over the 2-theta range, the instrument profile and the mineral structure parameters (Taut, et al., 1998). Rietveld refinement accounts for variations in mineral composition on peak position, as well as the effect of small size and strain on peak shape and area. Therefore, it is an ideal choice to quantify cement hydration products.

RESULTS AND DISCUSSION

Unconfined Compressive Strength (UCS)

The effects of biochar addition and biochar size on UCS of cement stabilized peat soil were compared to sand fillers (Fig. 1). The increase in UCS strength associated with biochar filler is comparable to that associated with sand. Most importantly, for biochar size smaller than 75 μm, cement stabilized peat UCS surpasses that of coarser biochar size filler by 170% and that of same grain-size sand by 35%. Fig. 1 shows that the biochar size effect starts in the early stages of hydration: it is already evident at 7 days. After 28 days, a peak in UCS strength is evident for the fine-size biochar. This is an unexpected result. Unconfined compressive strength in these mixes is due to the presence of cement that allows bonding of particles. Inert fillers add particles that the cement can bind to and together they create a stronger and stiffer structure within the matrix material. All specimens have equal amount by weight of cement, peat and either sand or biochar. Sand grains are harder than biochar, with reported hardness values of 10 GPa and 3 GPa,

160 respectively (Daphalapurkar, et al. 2010, Dixit, et al. 2019). In the composite material, we
161 expect failure surfaces to seek weak bonds, with less cement, or go through areas with a
162 less favorable distribution of cement. The relative greater hardness of sand grains than
163 biochar seems to favor sand because failure could occur through biochar grains whereas
164 it will always go around sand grains. This mechanism could explain the slightly higher
165 UCS associated with a sand filler for samples A to D. However, it does not explain the
166 higher strength of sample E with biochar filler of the finest size. Smaller particles appear
167 to provide a more uniformly distributed network to support the cement bonds, leaving
168 fewer weak uncemented spots, as both fine sand and fine biochar result in higher
169 strengths. However, this mechanistic interpretation cannot fully explain the large
170 difference between the two materials in favor of biochar.

171 As a porous material, biochar absorbs some water, but the overall availability for the
172 cement hydration reactions is far in excess of the optimum water/cement ratio. The water
173 content of all sand specimens at 28 days is in excess of 130% with higher values (>150%)
174 for the biochar specimens. The intra-group difference is minimal in each set, where
175 specimens A-D have nearly the same water content as specimen E.

176 **Scanning Electron Microscopy**

177 Our characterization of peat-biochar-OPC mixtures, at 7 days of hydration, is based on
178 the analysis of over 90 SEM-SE micrographs from air-dried samples, more than 140 SEM-
179 BSE micrographs (atomic contrast) from embedded-polished blocks and over 200 EDS

180 spectra.

181 Analysis by SEM reveals the presence of calcium silicate hydrate (C-S-H) and ettringite
182 needles in all samples (Fig. 2). C-S-H gel, easily identifiable from its sponge-like texture,
183 completely covers the grains whereas ettringite needles, up to 10 μm in length, protrude
184 from the gel. EDS analysis from a rectangular region of the coating (C 34 in Fig. 2) shows
185 O, Ca and Si, with lesser fraction of Al and traces of Mg which is consistent with the
186 chemical composition of C-S-H (Richardson 2008, L'Hôpital, et al. 2015). Similarly, EDS
187 from the needles (Point C33 in Fig. 2) shows the presence of O, Ca, Al and S, consistent
188 with ettringite, the most common sulfoaluminate phase (AFt). C-S-H and ettringite are
189 two major products of the early stages of cement hydration that form from the reaction
190 of tricalcium silicate (C_3S), calcium aluminate (C_3A) and gypsum with water.

191 Fragments of biochar are identified in SEM micrographs by their rigid, open cellular
192 structure, composed of a bundle of sub-prismatic cells, separated by solid walls (Fig. 3-
193 A, B). Measurements taken from polished sections (Fig.3-C) indicate that wall thickness
194 ranges between 1 and 3 μm, cell width between 7 and 10 μm and cell length between 20
195 and 40 μm. Fig. 3-A, B show the typical appearance of a biochar fragment after one week
196 of curing, with its surface covered by hydration products. C-S-H coating grows with a
197 sponge-like appearance on the surface and ettringite needles fill the cells, to varying
198 extent. Polished cross sections of the biochar, analyzed in backscatter mode (Fig. 3-C),
199 further show that filling of the cells is complete in the outer portion of the biochar and

200 decreases inward, with the innermost cells remaining void, or partially covered by a thin
201 layer of C-S-H. The composition of the filling also undergoes some changes as portlandite
202 (CH in cement notation) and other Ca compounds are only found in the outer cells,
203 whereas C-S-H tends to penetrate further inward (Fig. 3-C). For samples A to D, biochar
204 fragments still preserve their internal, cellular structure (Fig. S-1). Sample E, where
205 biochar size is smaller than 75 μm, is the exception, as most fragments are too small to
206 show any relict internal cells (Fig. S-1). Instead, biochar pieces appear as rigid particles
207 with complex, jagged shape and large, exposed surface area but no preserved internal
208 macro-pores.

209 Although peat fragments are heterogeneous in shape and size, they are always orders
210 of magnitude larger than cement particles and larger than biochar fragments. Like
211 biochar, many peat fragments show internal cells but, in contrast to biochar, peat
212 fragments are flexible, they look bent and deformed. In fact, many peat fragments appear
213 as porous ribbons that wrap cement and hydration products (Fig. 4). BSE micrographs
214 show that peat is commonly associated with larger voids and more porosity, distributed
215 both inside the peat (intraporosity) and between peat fragments.

216 In some instances (Fig. 4-D, Fig. S-2), cells within the peat show varying degrees of
217 filling by Ca-Al rich minerals and Ca-Al minerals with minor Si and S, as determined by
218 EDS.

219 In samples C, D, and E microcrystalline, microporous aggregates of calcite ($CaCO_3$), 5

220 to 20 μm in size are found, most frequently filling the outer cells of biochar, rarely outside
221 biochar fragments (Fig. 5).

222 The microcrystals are assembled in tight cubic grains that show growing bands in BSE
223 (Fig. 6), a clear evidence that they grew in situ. EDS analysis cannot effectively
224 differentiate portlandite and calcite. However, these two minerals have significantly
225 different average atomic number (calcite 12.56 and portlandite 14.3) because of their
226 different crystal structure, that results in different backscattered absorption coefficients
227 (calcite: 0.142, portlandite: 0.162) therefore different contrast in BSE micrographs
228 (Stutzman 2004). The difference in contrast was clear in our BSE analysis.

229 **Mineralogy after at 7 Days of Curing by XRD**

230 The 7 days XRD patterns of the mixtures with five different grain size of biochar and
231 the control sample show reflections at similar 2-theta angles and overall similar features.
232 The presence of peat contributes a diffuse reflection and also attenuates the reflection of
233 other minerals, adding complexity to the pattern (Fig. 7). Biochar fibers are composed of
234 both crystalline and amorphous material, with a degree of crystallinity reported in the
235 literature on the order of 40-60% (Borrega, et al. 2015). Biochar crystalline component is
236 primarily cellulose and is observed in the XRD pattern by its reflection at 22.9°2θ.
237 Portlandite, calcite and C_2S (larnite) account for the most intense and narrow peaks in the
238 XRD pattern (Fig. 7), indicating that these are the most abundant crystalline components
239 of the mixture. C_2S is a slow reacting clinker component that contributes to the long -term

240 strength of the cement and is expected to be found after 7 days. In contrast, the fast
241 reacting components of the clinker, gypsum, tricalcium silicate (C_3S), and calcium
242 aluminate (C_3A), were not detected either by XRD or SEM, indicating that the initial phase
243 of OPC hydration had completed.

244 CH, C-S-H and ettringite are the main products of hydration and among them, only
245 CH forms well developed crystals that yield clear peaks in the diffraction pattern.
246 Ettringite peaks are commonly identified in XRD patterns (Hernandez-Martinez 2006),
247 but are not visible in the XRD patterns of these samples, at 7 days or even at 28 days.
248 Nonetheless, needles with the morphology and chemical composition of ettringite were
249 observed by SEM, in all samples. The absence of peaks in the XRD pattern may be due to
250 the attenuating effect of peat, in combination with a low degree of crystallinity of
251 ettringite. C-S-H make up the main binding agent during the early hydration stage but
252 they are difficult to characterize and identify because their composition is variable and
253 they are generally poorly crystalline (Richardson 2008, Lothenbach and Winnefeld 2006).

254 The experimental diffraction patterns at 7 days show broad reflections on the shoulder
255 of C_2S peaks that can be attributed to C-S-H and specifically to rosenhanite (C_3S_3H) and
256 dellaite (C_6S_3H), depending on sample (Fig. 8).

257 The presence of calcite detected by XRD, and confirmed by SEM-BSE micrographs
258 (Fig. 5), is evidence that, in addition to the hydration reactions that lead to formation of
259 CH and C-S-H, carbonation also takes place. The carbonation reaction occurs when CO_2

diffuses into pore water and forms carbonic acid (H_2CO_3) which, in turn, dissociates into bicarbonate ion (HCO_3^-), and carbonate ion (CO_3^{2-}) causing the pH to decrease (Cizer, et al. 2012). The lower pH drives the reaction of portlandite with the carbonate ions in solution to form calcite and water, according to Eq. 1 (Johannesson and Utgenannt 2001, Cizer, et al. 2012, Frías and Goñi 2013, Shi, et al. 2016):

$$Ca(OH)_2 + CO_3^{2-} \rightarrow CaCO_3 + H_2O \quad (1)$$

The carbonation reaction in concrete is diffusion limited, it only occurs on surfaces exposed to a source of CO_2 (Haselbach 2009). Labile Carbon in peat is one source that has been shown to promote the carbonation reaction (Duggan, et al. 2019). SEM analysis demonstrate that another important source is biochar.

While it is considered inert, research shows that a transient flux of CO_2 can be released by biochar within the first few days to weeks after addition to soils (Cardelli, et al. 2016, Bruun, et al. 2014). It is quite likely that a similar release occurs from the surface of the biochar mixed to cement. Experimental studies show that carbonation of portlandite has negligible effect on pH (Shi, et al. 2016) because it is a surface process that proceeds only as deep as the reach of the diffusion of CO_2 and has a positive effect on strength, as long as the distribution of calcite is homogeneous (Cizer, et al. 2012). Negative effects on strength are possible when a carbonation front develops, as for CO_2 injection, leading to localized micro-crack formation (Fabbri, et al. 2009). This is not the case for our samples where instead biochar is homogeneously mixed with the peat and cement. Therefore, any

release of CO_2 from biochar surface, is also randomly distributed within the sample.

Another region of interest in the XRD pattern is between 6 − 25°2θ (Fig. 9). A diffuse but clear reflection occurs at a 2-theta angle of ~ 19°, in all samples that contain biochar. This peak indicates the presence of an AFm phase, a group hydrated layered calcium aluminate with general composition of $Al_2O_3 - Fe_2O_3 - X$, where X indicates a monocharge anion like OH^-, or half of a doubly charged anion like SO_4^{2-}, CO_3^{2-} (Matschei, Lothenbach and Glasser 2007). AFm phases can form from the hydration of C_3A, C_4AF or conversion of ettringite and C-S-H. The peaks in the XRD pattern can be attributed to monocarboaluminate, a phase that forms when excess Al and Ca occur with respect to sulfate (Bonavetti, Rahhal and Irassar 2001, Ipavec, et al. 2011).

Accordingly, calcite and carbonate ions favor the formation of monocarboaluminate, as well as the transient hemicarboaluminate (Ipavec, et al. 2011, Mohamed, et al., 2015). Thermodynamic modeling of cement hydration shows that monocarboaluminate is the most stable form of AFm (Lothenbach and Winnefeld 2006).

Early studies on the effect of monocarboaluminate on mechanical properties found that its formation did not negatively affect the strength, compared to other AFm phases (Fernández, et al., 2018, Lothenbach, et al. 2008). Moon et al. (2014) found a dependence between compressibility of monocarboaluminate with number of layers of water in the interlayer of the structure.

298 **Mineral Quantification by Rietveld Refinement at 7 Days of Curing**

299 An example result plot of the Rietveld refinement is shown in Fig. 10. The main graph
300 shows the experimental diffraction pattern (black) and the simulated pattern (magenta)
301 based the on the minerals identified. The bottom plot shows the difference between the
302 experimental and simulated profiles. Simulation of mineral XRD patterns is based on
303 atomic structure models taken either from the ICDD pdf-4 mineral database (Kabekkod
304 2016) or from the Crystallography Open Database (Grazǔlis, et al. 2012). The shape of
305 mineral peaks is modified by variables that depend on instrument settings, crystallite size
306 and mineral abundance. Cellulose is included in the mixture because it is a crystalline
307 component of biochar that can be identified in the experimental patterns. Table 2 lists the
308 mineral models used, and the results of the quantification, normalized to the crystalline
309 fraction of the mixture.

310 Table 2 groups clinker components and hydration products. Peat and biochar
311 contribute a diffuse reflection that is added to the background. It is evident, from the
312 quantification results, that the extent of hydration at 7 days, indicated by the sum of all
313 hydration products, is similar in all samples (Fig. 11). The composition of the hydrated
314 products however, changes between the control sample and the samples with biochar
315 filler. Calcite, while present in all samples, is far more abundant in samples with biochar,
316 a confirmation that carbonation occurs in OPC stabilized peat and is promoted by
317 biochar. Further, an inverse trend between the concentration of calcite and portlandite,

318 indicates carbonation of the latter.

319 Monocarboaluminate is another mineral that shows a significant variation in
320 abundance between the control sample, where it is not detected, and the samples with
321 biochar filler, containing 5 to 9%. While there is no obvious trend, sample E, with the
322 finest grain size, contains the largest fraction.

323 **Mineralogy Changes Over Time**

324 Diffraction patterns collected after 28 days of hydration from samples A and E, the two
325 end members of biochar grain size subdivisions, show identical features (Fig. 12). The
326 similarity in mineralogy is evidence that the hydration reaction proceeds towards the
327 same end composition over time, in all samples with biochar filler. Size, therefore, is
328 important in the early stages when hydrated minerals nucleate on the surface of biochar.
329 This result is consistent with research by Dixit et al. (2019) who observed an acceleration
330 of the hydration reaction after adding fine-size (<150 μm) biochar to OPC. Dixit et al.
331 (2019) found that coarser-size biochar promoted hydration in later stages, due to slow
332 moisture release. Not surprisingly, this is not the case in our study where specimens
333 could take in water, during curing.

334 The long-term trend of the mineralogy of the OPC stabilized samples with filler was
335 assessed from sample E, by quantitative mineral analysis at 7, 28 and 120 days. Mineral
336 quantification, normalized to the crystalline fraction, is shown in Table 3 while the bar
337 diagrams in Fig. 12 display the trend of the hydrated minerals. The results show that

monocarboaluminate persists in the long terms, and its concentration increases over time. Further, the full-width at half maximum of this mineral XRD peak becomes narrower, indicating an increase in the size of diffracting domain -that reflects larger and more ordered crystals. Notably, the content of calcite also shows a distinct increase over time, up to 40 % of the mineral fraction. This further confirms that carbonation contributes to the increase in strength of the material.

Portlandite concentration also increases in the long term. However, it suffers a transient decrease in concentration at 28 days, concomitant with the occurrence of two calcium oxalate salts (Ca-oxalate and Ca-oxalate hydrate). These salts, that give sharp peaks in the XRD pattern at 13, 14, 19°2θ (Fig. 12), precipitate from humic acids in the presence of excess calcium (Franceschi and Nakata 2005). Likely, the excess calcium is released by dissolution of portlandite whereas humic acids derive from the peat, biochar, or both. Such dissolution can occur from a local lowering of the pH associated with the progression of the carbonation reaction (Johannesson and Utgenannt 2001).

In mixtures, Ca-oxalate is, however, a transient phase that is fully consumed between 28 and 120 days. In fact, the diffraction pattern of sample E, after 120 days of hydration, does not show any Ca-oxalate peaks (Fig. 12). Rather, the concentration of portlandite increases from approximately 6 % to 23 % between 28 and 120 days, raising above the 7 days concentration (Fig. 13). Calcite concentration decreases slightly from 39 % to 32 % while C-S-H concentration increases but at slower pace than in the first 7 days. During

358 the same time, the abundance of the unreacted clinker (C_2S) decreases from
359 approximately 24 % to 16 % (Table 3). Clearly, over time, the remaining clinker
360 components in OPC hydrate, buffering any local change in pH, and yield mineral phases
361 that add strength to the peat. In fact, UCS tests show calcite, portlandite and
362 monocarboaluminate are the minerals that contribute to the overall strength.

363 **Texture and Microstructure**

364 SEM-BSE micrographs of the control sample, which is solely composed of peat and
365 OPC, show clusters composed of a core of unreacted C_4AF and C_2S, with sub-round shape
366 and average size of 25 μm that is surrounded by C-S-H gel and ettringite. These clusters
367 are dispersed in the matrix, with relatively homogeneous distribution (Fig. 14 A, B). Peat
368 fragments with heterogeneous morphology and size also show a relatively homogeneous
369 spatial distribution. Void space is still dominant after one week. In fact, measurements
370 from image analysis of BSE micrographs show that at least 50 % of the area fraction is
371 void space, with the largest voids found in peat chambers and along the rim of peat
372 fragments (Fig. 14-B). As the clusters of cement and hydration products grow, they fill in
373 the void space, displace and deform the peat. The size of clusters and their hydration
374 shells vary by location, indicating local variability in extent of hydration, at this stage.

375 With the addition of biochar, hydration of cement not only occurs in clusters located
376 in the void space of the mixture, but also, and more importantly, on the external surface
377 and cells of biochar. Fig. 3 showed that the biochar surface catalyzes the nucleation of C-

S-H and AFm phases. BSE micrographs show a rind of cementitious gels at the outer edge of large biochar fragments (Fig. 14-C, D) and the edges of fine fragments (Fig. 14-E). Coated biochar edges appear brighter. BSE micrographs further show that hydration products do not reach the inner cells of large biochar fragments, likely because the newly formed hydration products tend to occlude pores and pore throats. In contrast to peat, biochar fragments are rigid therefore offer higher resistance to deformation, leading to an increase in strength of the overall mixture.

At this early stage however, rigid biochar bodies are still separated by large void space that provides weak zones where fractures can develop and grow. In larger fragments (Fig. 14-C, D) weak surfaces are also larger. Further, in samples A through D it is common to observe clusters of biochar fragments partially cemented together (Fig. 14-D) creating even larger weak surfaces around them. However, fragments of biochar that are sufficiently small to be comparable to the size of unhydrated cement grain, like in sample E, result in a homogeneous size distribution of the rigid grains in the mixture. In turn, the distribution of the granular, rigid material is also more homogeneous and less likely to favor development of weak surfaces.

Because the exposed surface of biochar promotes nucleation of hydrated products, a more homogeneous distribution of biochar also corresponds to a better distribution of hydration products. This better distribution is apparent in BSE micrographs from a comparison of samples with coarse fragments of biochar (Fig. 14-C, D) with sample E

(Fig. 14-E, F). According to this hypothesis, as hydration progresses, the new hydrated minerals will progressively fill the void space, deform and compress the peat, ultimately yielding a more continuous grain framework with more points of contact between particles, aggregates and biochar fragments.

CONCLUSIONS

As sand becomes less available and more expensive, alternatives that are both sustainable and environmentally friendly are highly desirable. Biochar, the carbon negative product of pyrolysis, has been shown as a viable option to replace sand fillers in OPC stabilized peat soils (Lau et al., 2019). This paper investigated the mechanisms by which the addition of biochar contributes to the development of strength. Mineral, textural and microstructural characterization of cement stabilized peat soil samples with biochar filler demonstrated that 1) biochar catalyzes the nucleation of hydration minerals on its surface. 2) It favors hydration reactions that encourage the formation of minerals that add strength to the peat, in the short and long term. 3) Biochar counteracts the negative effects of peat on cement hydration. 4) Similarly to sand filler, the microstructure of the peat soil is improved by addition of rigid grains to an otherwise soft and easily deformable material. 5) A particle size smaller than 75 μm results in better filling of the space by biochar. In turn, the more biochar surface becomes available to growth of hydration products, promoting faster rate of unconfined compressive strength increase in the early stages. Lastly, biochar favors the carbonation reaction, which contributes to

store carbon in a recalcitrant form.

Data Availability Statement

Some or all data, models, or code that support the findings of this study are available from the corresponding author upon reasonable request.

Acknowledgments

The authors thank three anonymous reviewers for their insightful and constructive comments. This work used shared facilities at the Virginia Tech National Center for Earth and Environmental Nanotechnology Infrastructure (NanoEarth), a member of the National Nanotechnology Coordinated Infrastructure (NNCI), supported by NSF (ECCS 1542100).

REFERENCES

ASTM 2013. Standard test method for unconfined compressive strength of cohesive soil. ASTM D2166. West Conshohocken, PA: ASTM.

Bonavetti, V. L., V. F. Rahhal, and E. F. Irassar. 2001. "Studies on the carboaluminate formation in limestone filler-blended cements." *Cement and Concrete Research* 31: 853-859. doi:10.1016/S0008-8846(01)00491-4.

Borrega, M., P. Ahvenainen, R. Serimaa, and L. J. Gibson. 2015. "Composition and structure of balsa (Ochroma pyramidale) wood." *Wood Science and Technology* 49: 403–420. doi:10.1007/s00226-015-0700-5.

Bruun, S., S. Clauson-Kaas, L. Bobuľská, and I. K. Thomsen. 2014. "Carbon dioxide emissions from biochar in soil: role of clay, microorganisms and carbonates." *European Journal of Soil*

Science 65: 52–59. doi:10.1111/ejss.12073.

Cardelli, R., M. Becagli, F. Marchini, A. Saviozzi, and M. Goss. 2016. "Short-term releases of CO2 from newly mixed biochar and calcareous soil." *Soil use and Management* 32: 543-545.

Cizer, Özlem, Carlos Rodriguez-Navarro, Encarnación Ruiz-Agudo, Jan Elsen, Dionys Van Gemert, and Koenraad Van Balen. 2012. "Phase and morphology evolution of calcium carbonate precipitated by carbonation of hydrated lime." *Journal of Materials Science* 47: 6151–6165. doi:10.1007/s10853-012-6535-7.

Daphalapurkar, N. P., F. Wang, B. Fu, H. Lu, and R. Komanduri. 2010. "Determination of Mechanical Properties of Sand Grains by Nanoindentation." *Experimental Mechanics* (Springer Science and Business Media LLC) 51: 719–728. doi:10.1007/s11340-010-9373-z.

Dixit, Anjaneya, Souradeep Gupta, Sze Dai Pang, and Harn Wei Kua. 2019. "Waste Valorisation using biochar for cement replacement and internal curing in ultra-high performance concrete." *Journal of Cleaner Production* 238: 117876. doi:10.1016/j.jclepro.2019.117876.

Döbelin, N., and R. Kleeberg. 2015. "Profex: a graphical user interface for the Rietveld refinement program BGMN." *Journal of Applied Crystallography* 48: 1573-1580. doi:10.1107/s1600576715014685.

Duggan, Alan R., Bryan A. McCabe, Jamie Goggins, and Eoghan Clifford. 2019. "Evidence of Stabilized Peat as a Net Carbon Sink." *Journal of Materials in Civil Engineering* 31: 04019005. doi:10.1061/(asce)mt.1943-5533.0002605.

Ellis, E. A. 2006. "Solutions to the problem of substitution of ERL 4221 for vinyk cyclohexene dioxide in Spurr low viscosity embedding formulations." *Microscopy Today* 14: 32-33. doi:10.1017/S1551929500050252.

Fabbri, A., J. Corvisier, A. Schubnel, F. Brunet, B. Goffé, G. Rimele, and V. Barlet-Gouédard. 2009. "Effect of carbonation on the hydro-mechanical properties of Portland cements." *Cement and Concrete Research* 39: 1156-1163. doi:10.1016/j.cemconres.2009.07.028.

Fernández, A., G. Calvo, and M. C. Alonso. 2018. "Ordinary Portland Cement composition for the optimization of the synergies of supplementary cementitious materials of ternary binders in hydration processes." *Cement and Concrete Composites* 89: 238-250. doi:10.1016/j.cemconcomp.2017.12.016.

Franceschi, V., and P. Nakata. 2005. "CALCIUM OXALATE IN PLANTS: Formation and Function." *Annual Review of Plant Biology* 56: 41-71. doi:10.1146/annurev.arplant.56.032604.144106.

Frías, Moisés, and Sara Goñi. 2013. "Accelerated carbonation effect on behaviour of ternary Portland cements." *Composites Part B: Engineering* 48: 122-128. doi:10.1016/j.compositesb.2012.12.008.

Gibson, L. J. 2003. "Cellular Solids." *MRS Bulletin* (Cambridge University Press (CUP)) 28: 270-274. doi:10.1557/mrs2003.79.

Gražulis, S., A. Daškevič, A. Merkys, D. Chateigner, L. Lutterotti, M. Quirós, N. R. Serebryanaya, P. Moeck, R. T. Downs, and A. Le Bail. 2012. "Crystallography Open Database (COD): an open-access collection of crystal structures and platform for world-wide collaboration." *Nucleic Acids Research* 40: D420-D427. doi:10.1093/nar/gkr900.

Gupta, Souradeep, and Harn Wei Kua. 2017. "Factors Determining the Potential of Biochar As a Carbon Capturing and Sequestering Construction Material: Critical Review." *Journal of Materials in Civil Engineering* 29: 04017086. doi:10.1061/(ASCE)MT.1943-5533.0001924.

Gupta, Souradeep, Harn Wei Kua, and Hui Jun Koh. 2018. "Application of biochar from food and wood waste as green admixture for cement mortar." *Science of The Total Environment* 619-620: 419–435. doi:10.1016/j.scitotenv.2017.11.044.

Hartlén, J., and W. Wolski. 1996. *Embankments on organic soils.* doi:10.1016/s0165-1250(96)80003-4.

Haselbach, Liv. 2009. "Potential for Carbon Dioxide Absorption in Concrete." *Journal of Environmental Engineering* 135: 465-472. doi:10.1061/(asce)ee.1943-7870.0000004.

Hernandez-Martinez, F.-G. 2006. "Ground Improvement of Organic Soils Using Wet Deep Soil Mixing." Ph.D. dissertation, Engineering Department, Cambridge University, UK, 331. doi:10.1016/b978-0-12-408076-8.00006-6.

Ipavec, A., R. Gabrovšek, T. Vuk, V. Kaučič, J. Maček, and A. Meden. 2011. "Carboaluminate Phases Formation During the Hydration of Calcite-Containing Portland Cement." *Journal of the American Ceramic Society* 94: 1238–1242. doi:10.1111/j.1551-2916.2010.04201.x.

Janz, M., and S.-E. Johansson. 2002. "The Function of Different Binding Agents in Deep Stabilisation, Report 9." *The Function of Different Binding Agents in Deep Stabilisation, Report 9.* Swedish Deep Stabilization Research Centre. 1–50.

Johannesson, Björn, and Peter Utgenannt. 2001. "Microstructural changes caused by carbonation of cement mortar." *Cement and Concrete Research* 31: 925-931. doi:10.1016/S0008-8846(01)00498-7.

Kabekkod, Soorya, ed. 2016. "PDF-4+ 2016." *PDF-4+ 2016.* ICDD (International Centre for Diffraction Data). doi:10.18411/d-2016-154.

Larson, C. 2018. "Asia's hunger for sand takes toll on ecology." *Science* 359: 964-965.

doi:10.1126/science.359.6379.964.

Lau, J., G. Biscontin, and D. Berti. 2019. "Effects of biochar on cement stabilised peat soil." *Proceedings of the Institution of Civil Engineers Ground Improvement* 1–12. doi:10.1680/jgrim.19.00013.

Lehmann, J., and S. Joseph, . 2015. *Biochar for Environmental Management.* Taylor & Francis. doi:10.4324/9780203762264.

L'Hôpital, E., B. Lothenbach, G. Le Saout, D. Kulik, and K. Scrivener. 2015. "Incorporation of aluminium in calcium-silicate-hydrates." *Cement and Concrete Research* 75: 91-103. doi:10.1016/j.cemconres.2015.04.007.

Lothenbach, B., and F. Winnefeld. 2006. "Thermodynamic modelling of the hydration of Portland cement." *Cement and Concrete Research* 36: 209-226. doi:10.1016/j.cemconres.2005.03.001.

Lothenbach, B., G. Le Saout, E. Gallucci, and K. Scrivener. 2008. "Influence of limestone on the hydration of Portland cements." *Cement and Concrete Research* 38: 848-860. doi:10.1016/j.cemconres.2008.01.002.

Matschei, T., B. Lothenbach, and F. P. Glasser. 2007. "The AFm phase in Portland cement." *Cement and Concrete Research* 37: 118-130. doi:10.1016/j.cemconres.2006.10.010.

Mohamed, Ashraf Ragab, Mona Elsalamawy, and Marwa Ragab. 2015. "Modeling the influence of limestone addition on cement hydration." *Alexandria Engineering Journal* 54: 1-5. doi:10.1016/j.aej.2014.11.004.

Moon, J., S. Yoon, R. M. Wentzcovitch, and P. J. M. Monteiro. 2014. "First-principles elasticity of monocarboaluminate hydrates." *American Mineralogist* 99: 1360-1368.

527 doi:10.2138/am.2014.4597.

528 Osman, K. T. 2018. "Management of soil problems." Chap. Peat Soils, 145-183. doi:10.1007/978-3-
529 319-75527-4_1.

530 Park, J. H., G. k. Choppala, N. S. Bolan, J. W. Chung, and T. Chuasavathi. 2011. "Biochar reduces
531 the bioavailability and phytotoxicity of heavy metals." *Plant and Soil* 348: 439–451.
532 doi:10.1007/s11104-011-0948-y.

533 Qian, Kezhen, Ajay Kumar, Hailin Zhang, Danielle Bellmer, and Raymond Huhnke. 2015.
534 "Recent advances in utilization of biochar." *Renewable and Sustainable Energy Reviews* 42: 1055-
535 1064. doi:10.1016/j.rser.2014.10.074.

536 Richardson, I. G. 2008. "The calcium silicate hydrates." *Cement and Concrete Research* 38: 137-158.
537 doi:10.1016/j.cemconres.2007.11.005.

538 Shi, Zhenguo, Barbara Lothenbach, Mette Rica Geiker, Josef Kaufmann, Andreas Leemann,
539 Sergio Ferreiro, and Jørgen Skibsted. 2016. "Experimental studies and thermodynamic
540 modeling of the carbonation of Portland cement, metakaolin and limestone mortars." *Cement*
541 *and Concrete Research* 88: 60-72. doi:10.1016/j.cemconres.2016.06.006.

542 Stutzman, P. 2004. "Scanning electron microscopy imaging of hydraulic cement microstructure."
543 *Cement and Concrete Composites* 26: 957-966. doi:10.1016/j.cemconcomp.2004.02.043.

544 Tan, Xiaofei, Yunguo Liu, Guangming Zeng, Xin Wang, Xinjiang Hu, Yanling Gu, and
545 Zhongzhu Yang. 2015. "Application of biochar for the removal of pollutants from aqueous
546 solutions." *Chemosphere* 125: 70-85. doi:10.1016/j.chemosphere.2014.12.058.

547 Taut, T., R. Kleeberg, and J. Bergmann. 1998. "The new Seifert Rietveld program BGMN and its
548 application to quantitative phase analysis." Edited by H. Morawiec and D. Stroz. *Proocedings of*

the XVII international conference. 87-92.

Tremblay, H., J. Duchesne, J. Locat, and S. Leroueil. 2002. "Influence of the nature of organic compounds on fine soil stabilization with cement." *Canadian Geotechnical Journal* 39: 535–546. doi:10.1139/t02-002.

Wang, Lei, Liang Chen, Daniel C. W. Tsang, Binglin Guo, Jian Yang, Zhengtao Shen, Deyi Hou, Yong Sik Ok, and Chi Sun Poon. 2020. "Biochar as green additives in cement-based composites with carbon dioxide curing." *Journal of Cleaner Production* 258. doi:10.1016/j.jclepro.2020.120678.

Woolf, D., J. E. Amonette, A. Street-Perrot, J. Lehman, and S. Joseph. 2010. "Sustainable biochar to mitigate global climate change." *Nature Communications* 1: 1-9. doi:10.1038/ncomms1053.

Zhao, Sheng, Baoshan Huang, and Philip Ye. 2014. "Laboratory evaluation of asphalt cement and mixture modified by bio-char produced through fast pyrolysis." *Pavement Materials, Structures, and Performance.* American Society of Civil Engineers. doi:10.1061/9780784413418.015.

List of Tables

TABLE 1. Grain size of biochar used as filler.

Sample ID	Biochar size range
A	2.0 mm - 5.0 mm
B	425 µm - 2 mm
C	250 µm - 425 µm
D	75 µm - 250 µm
E	< 75 µm
Control	0

TABLE 2. Results of Rietveld on XRD patterns at 7 days

Mineral	**Control**	**A**	**B**	**C**	**D**	**E**
Hydration products						
Portlandite	19.9	8.49	9.86	16.7	22.6	13.6
Calcite	12.25	19	18.8	17.6	19.2	18.8
C-S-H	16.6	13.5	13.4	15.9	12.3	11.4
Monocarboaluminate	0.0	5.3	5.3	6.4	4.4	6.2
Cement paste						
C_2S	41.1	34	35.2	34.3	28.3	38.1
C_4AF	3.4	1.2	8.4	5.6	9.6	3.0
Other components						
Quartz	3.8	1.2	1.4	0.9	0.8	2.0
Cellulose	0	5.0	5.9	2.5	1.6	5.8

TABLE 3. Rietveld refinement of sample E XRD patterns 7, 28 and 120 days.

Mineral	**7 Days**	**28 Days**	**120 days**
Hydration products			
Portlandite	13.6	5.7	23.2
Calcite	18.8	39	32.2
C-S-H	11.4	5.6	9.7
Monocarboaluminate	6.2	8.1	6.3
Cement paste			
C_2S	38.1	24.3	16.0
C_4AF	3.0	4.3	4.9

Figure 1

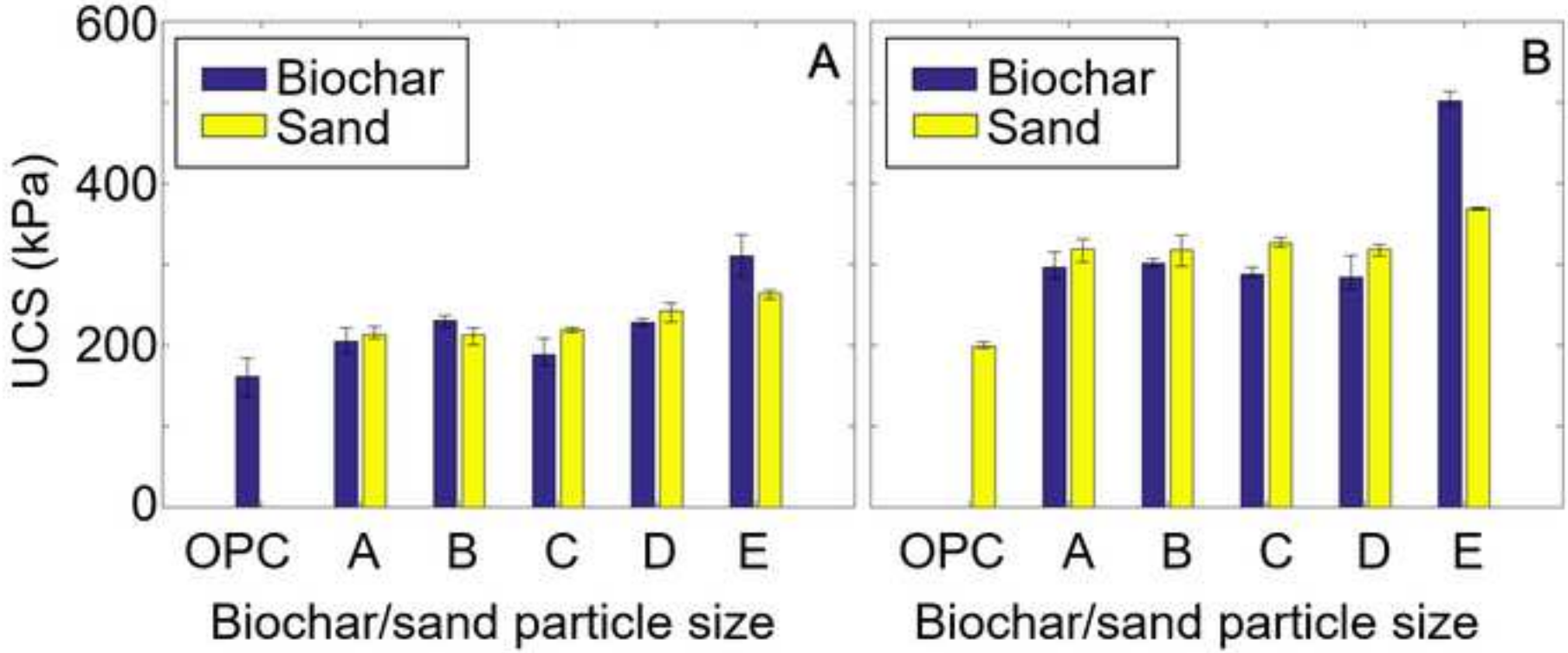

Figure 2

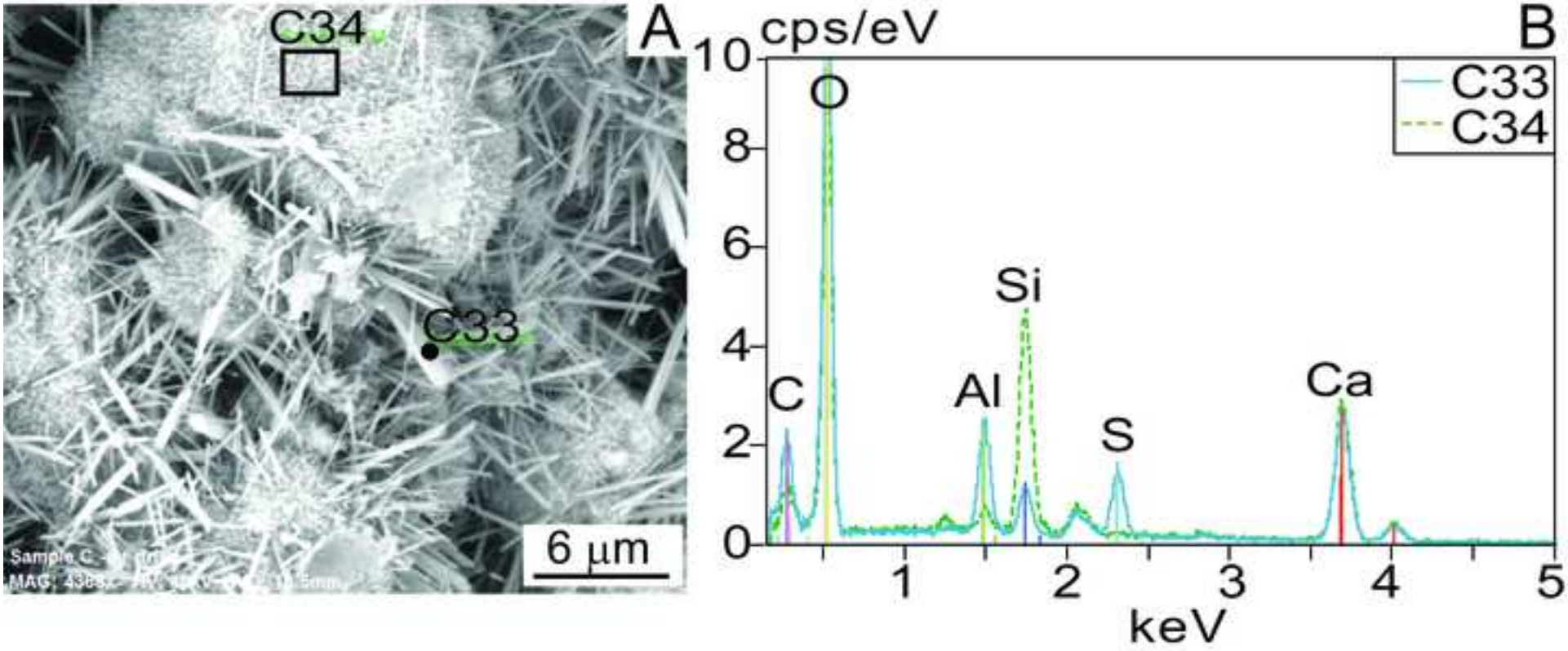

Figure 3

Click here to access/download;Figure;Fig3.tif

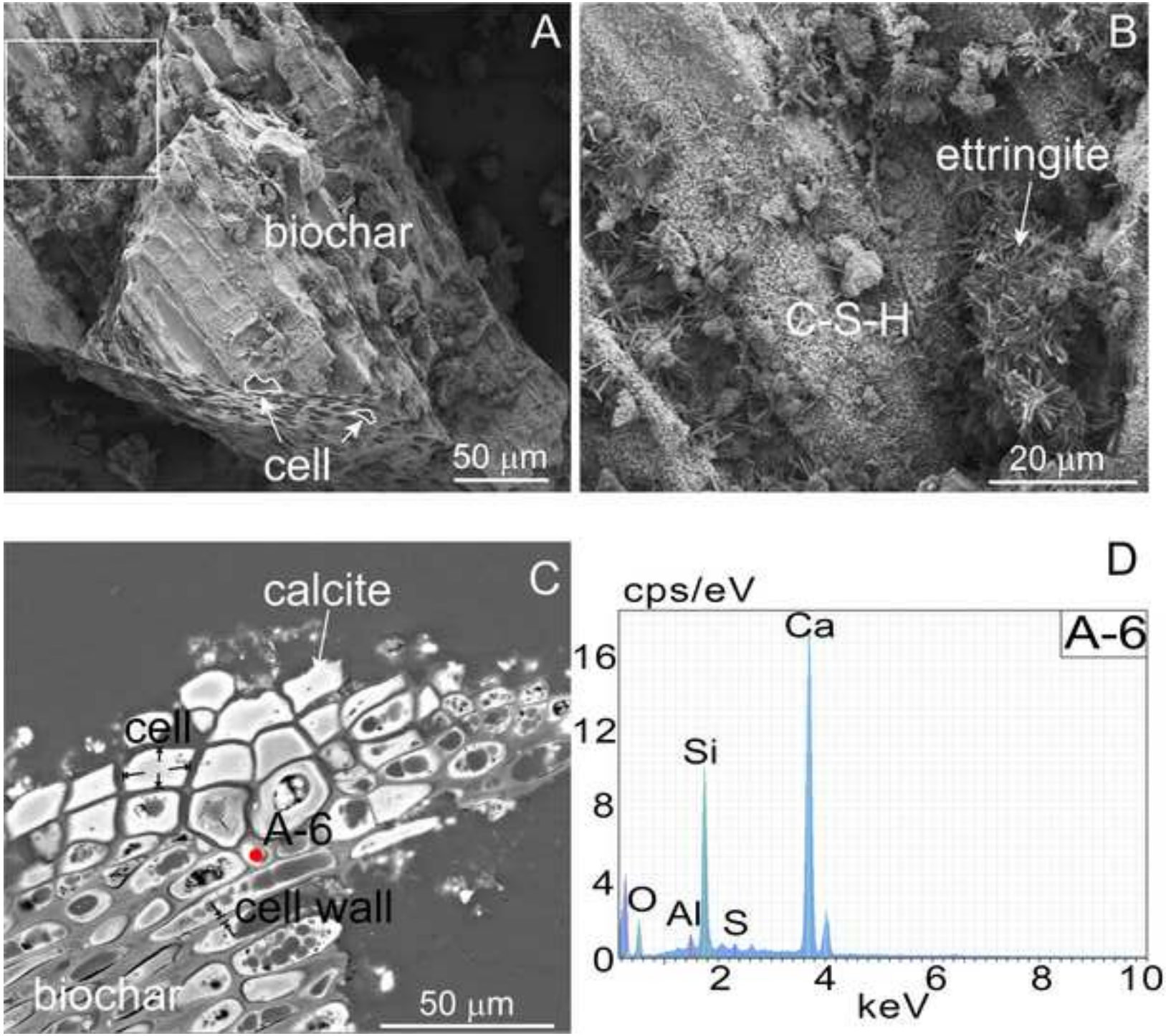

Figure 4

Click here to access/download;Figure;Fig4.tif

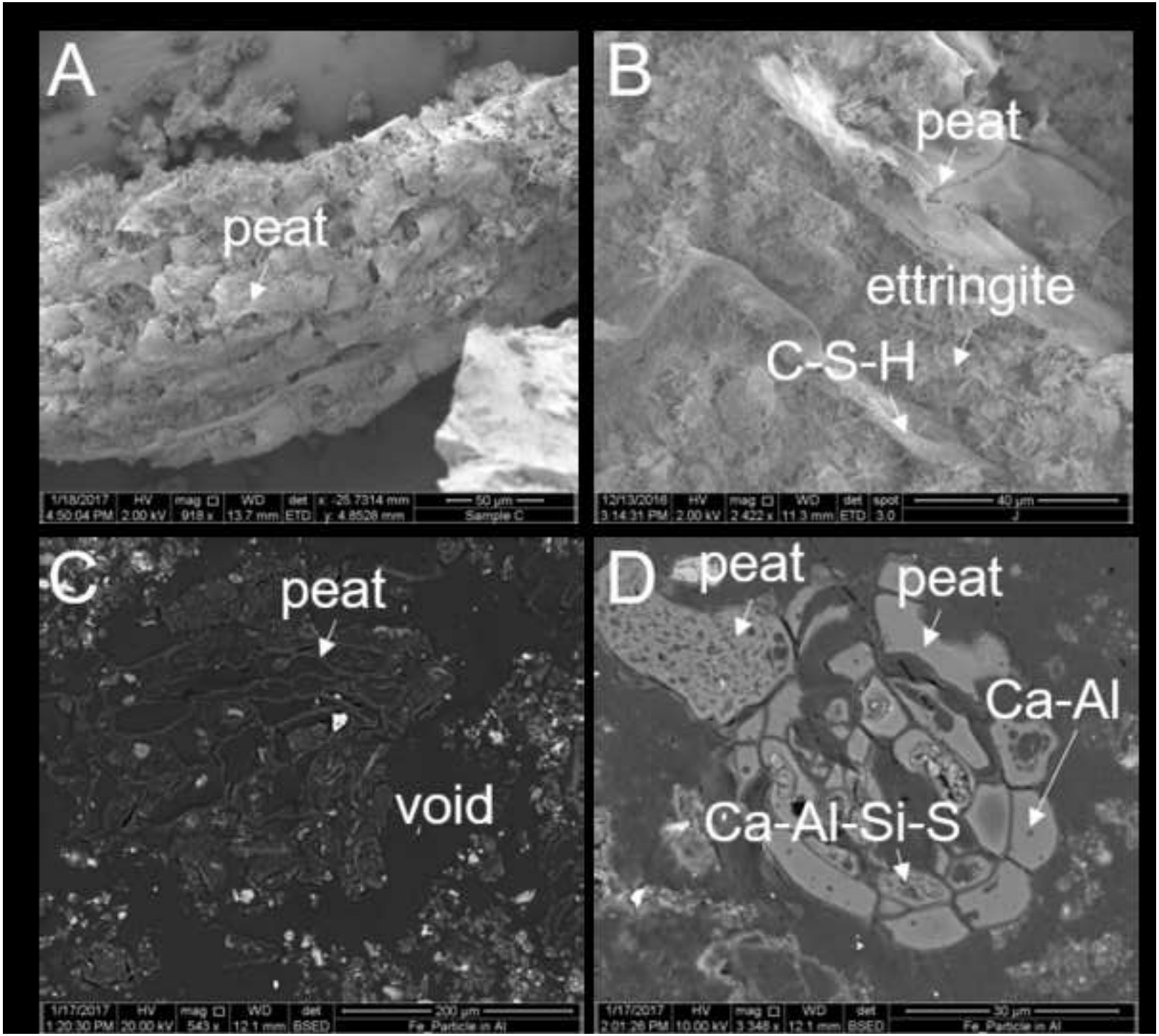

Figure 5

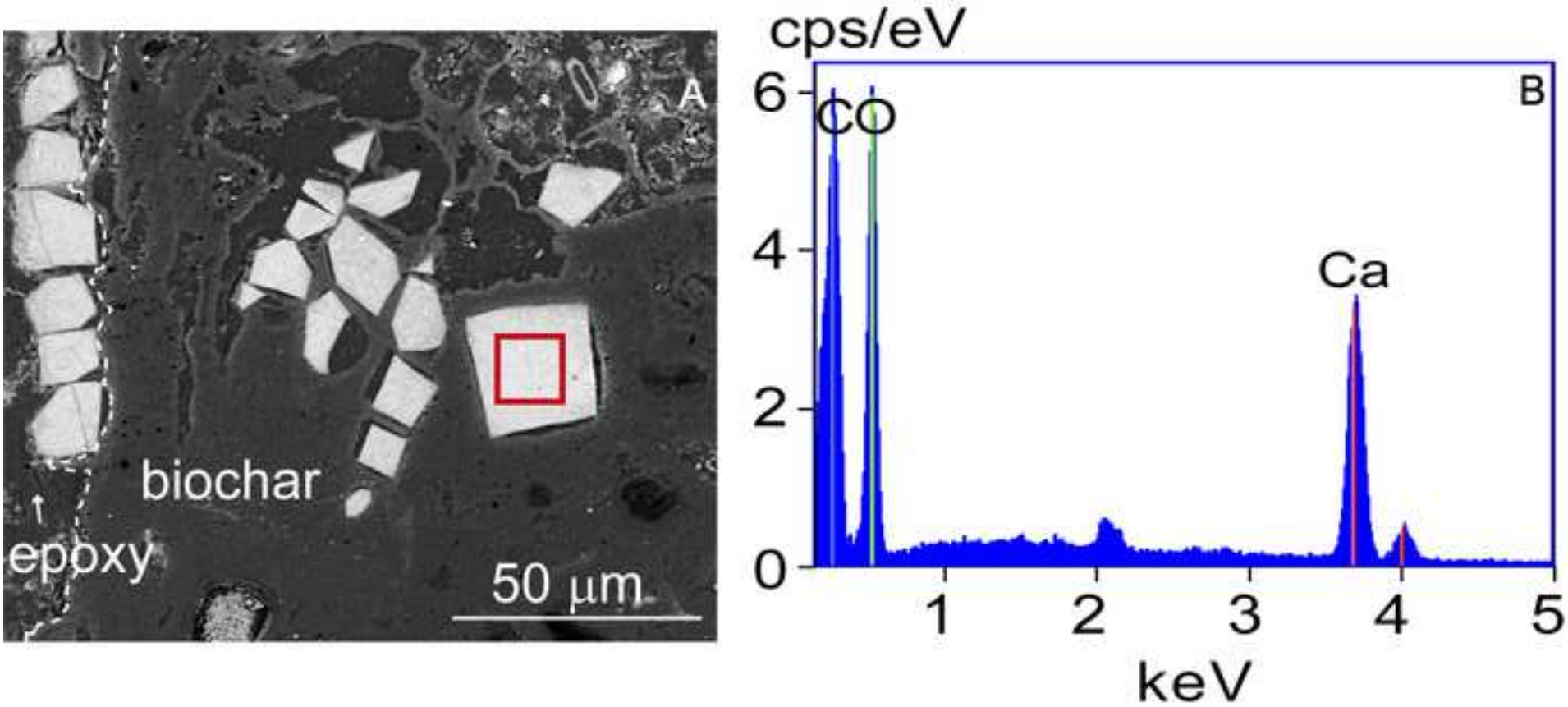

Figure 6

Click here to access/download;Figure;Fig6.tif

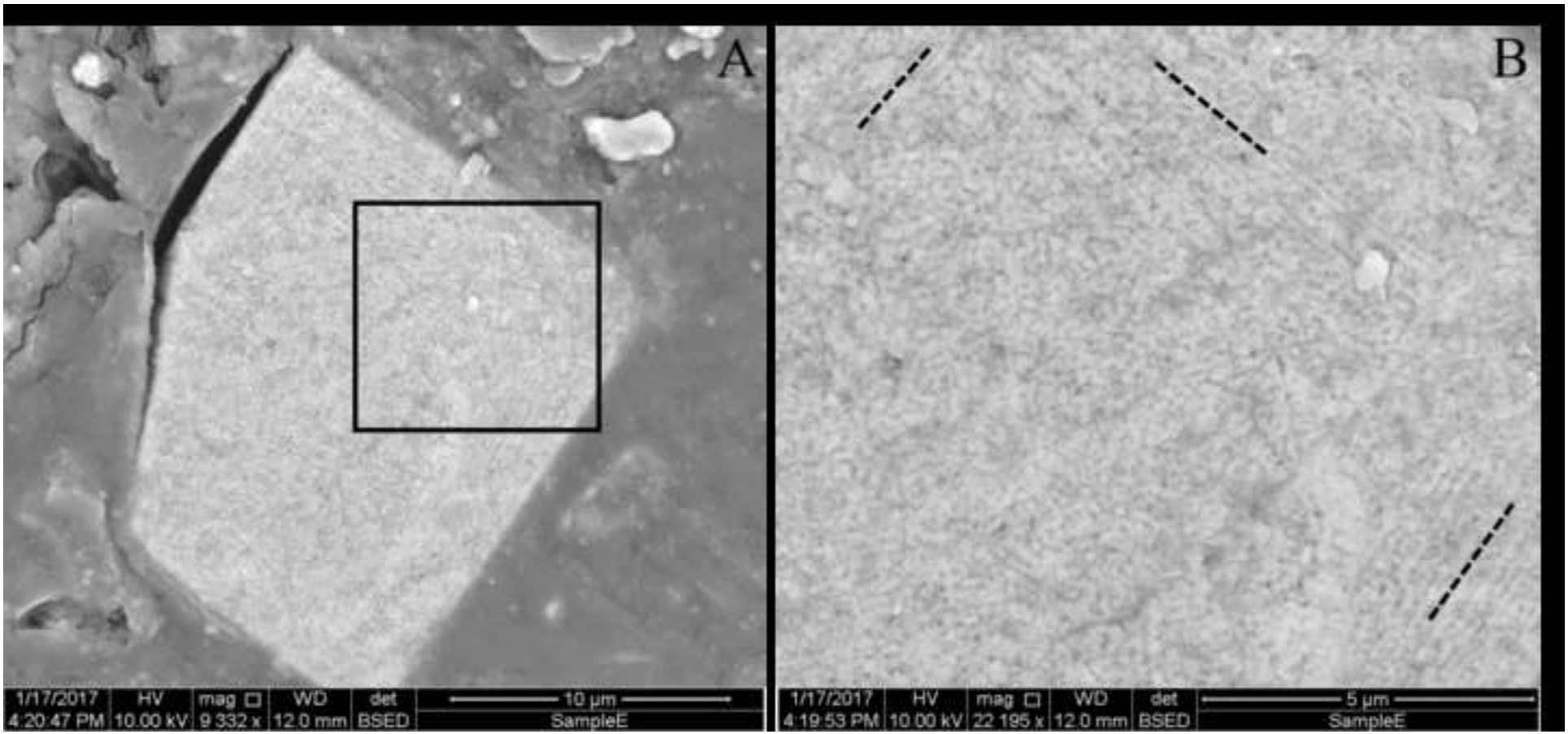

Figure 7

Click here to access/download;Figure;Fig7.tif

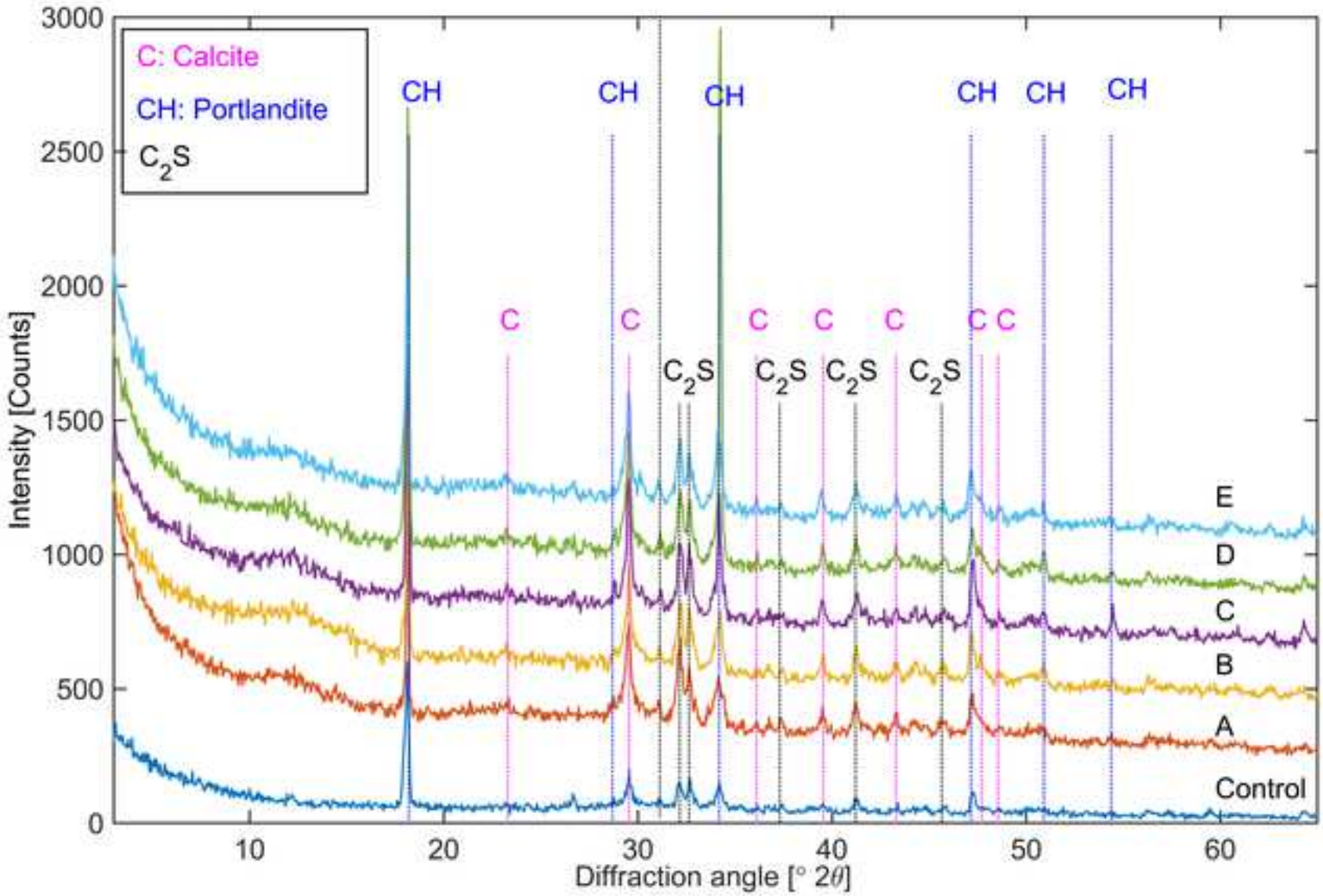

Figure 8

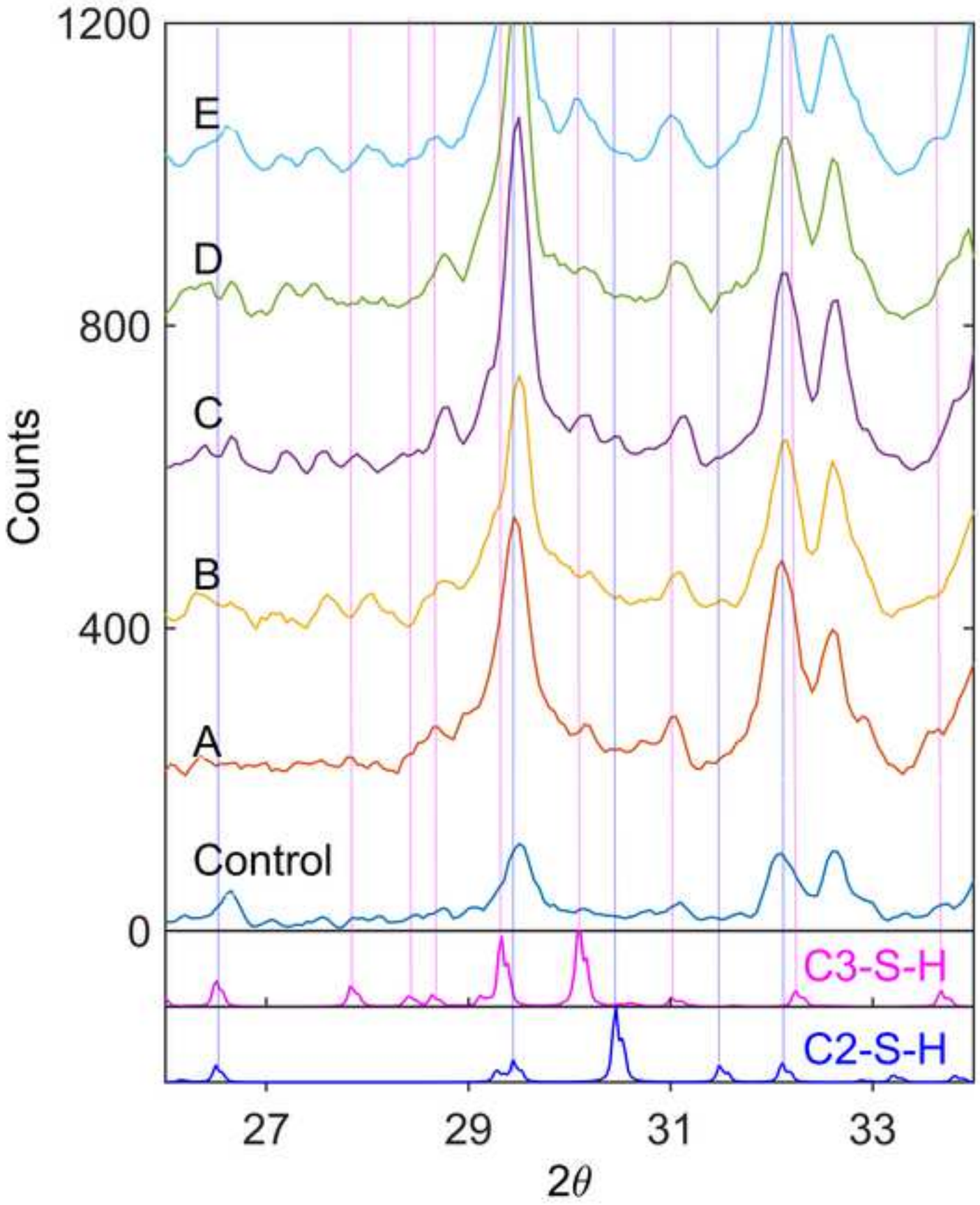

Figure 9

Click here to access/download;Figure;Fig9.tif

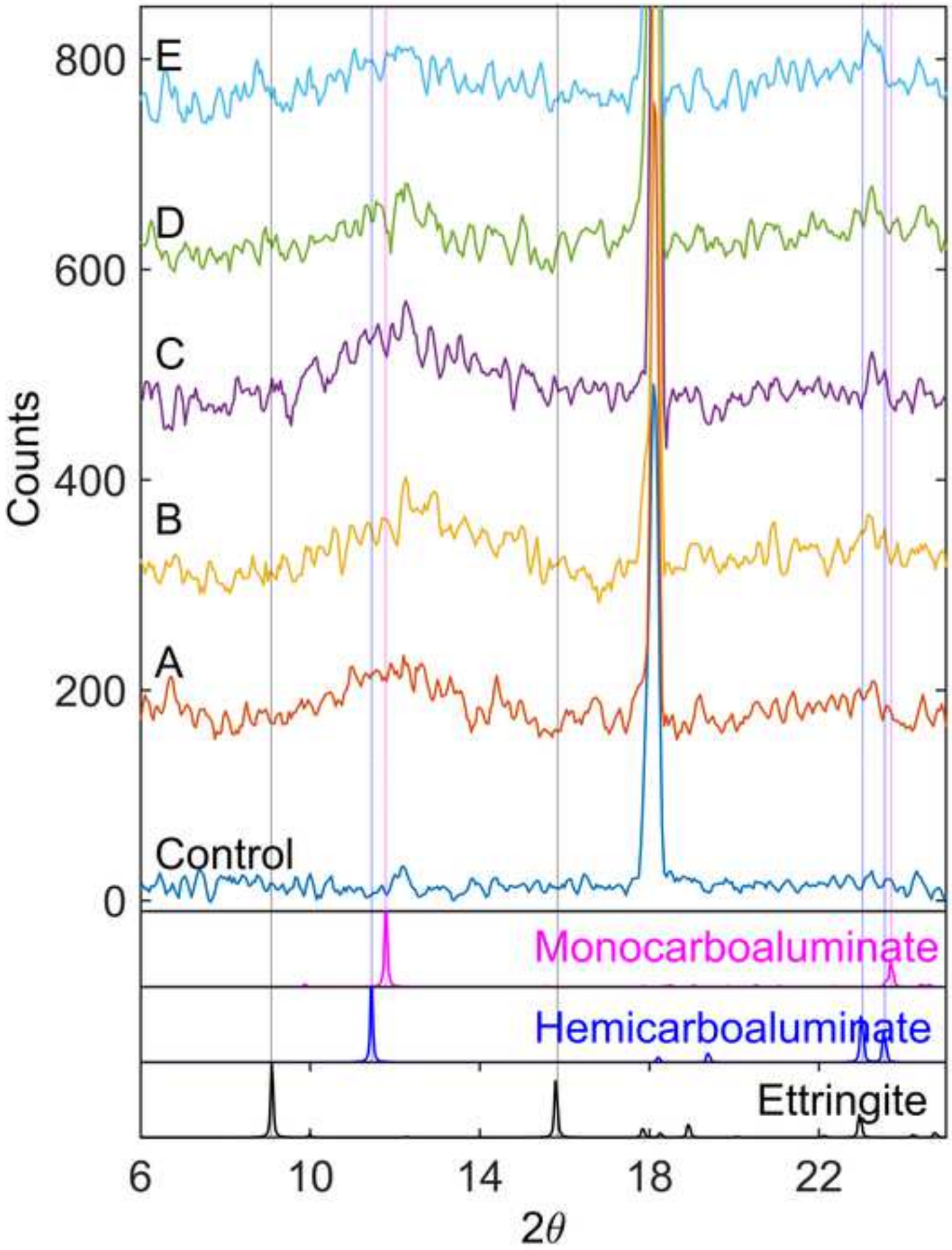

Figure 10

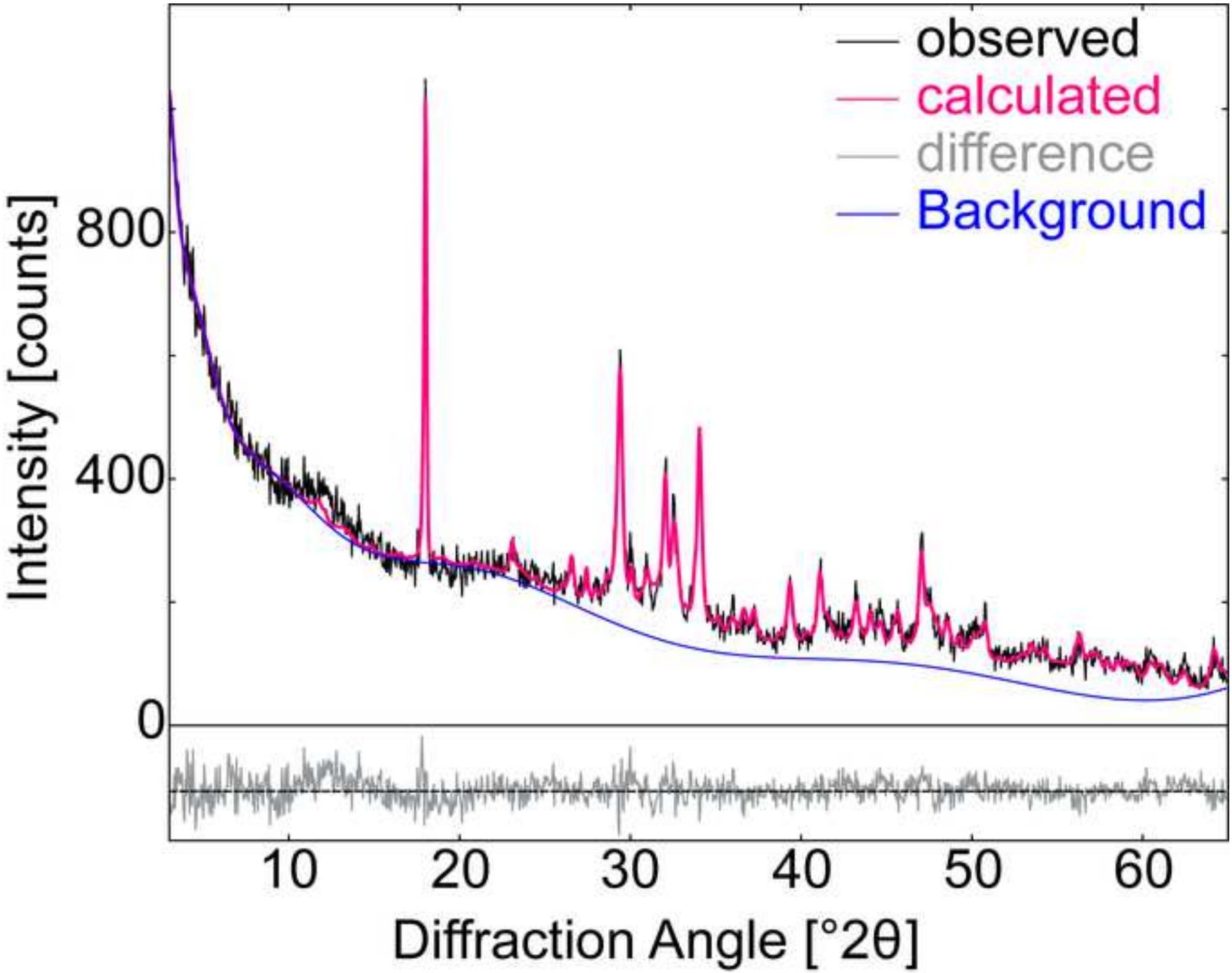

Figure 11

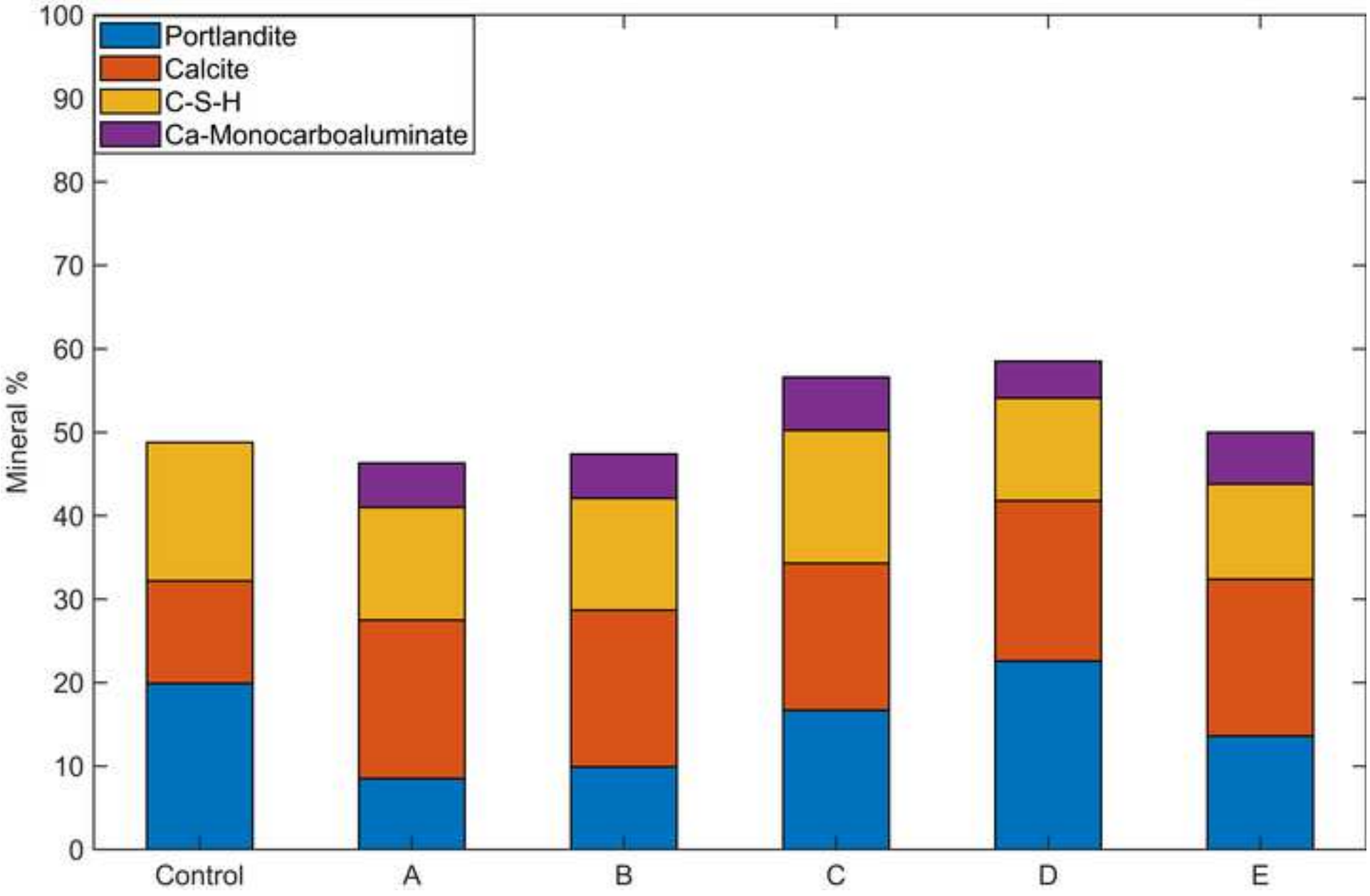

Figure 12

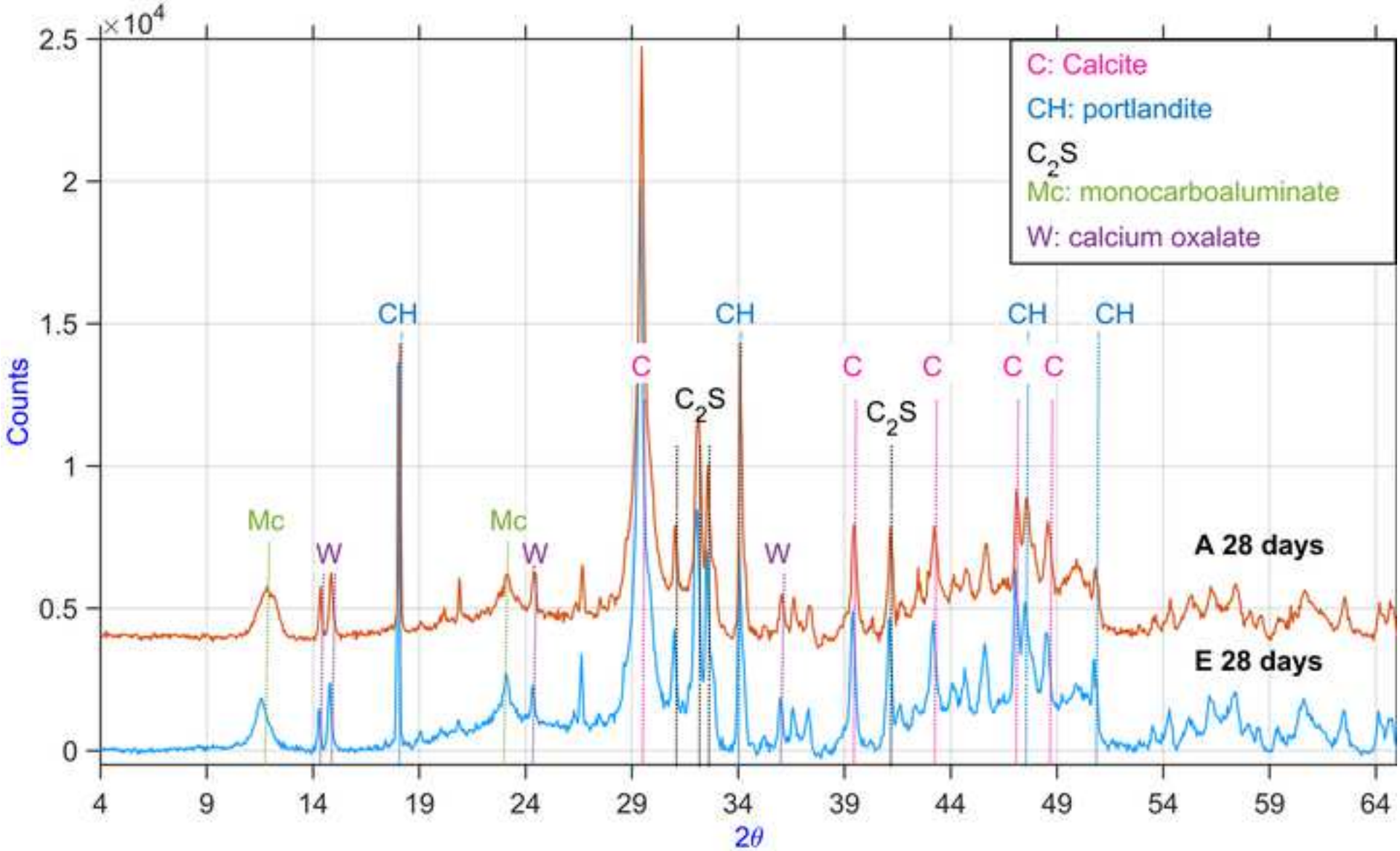

Figure 13

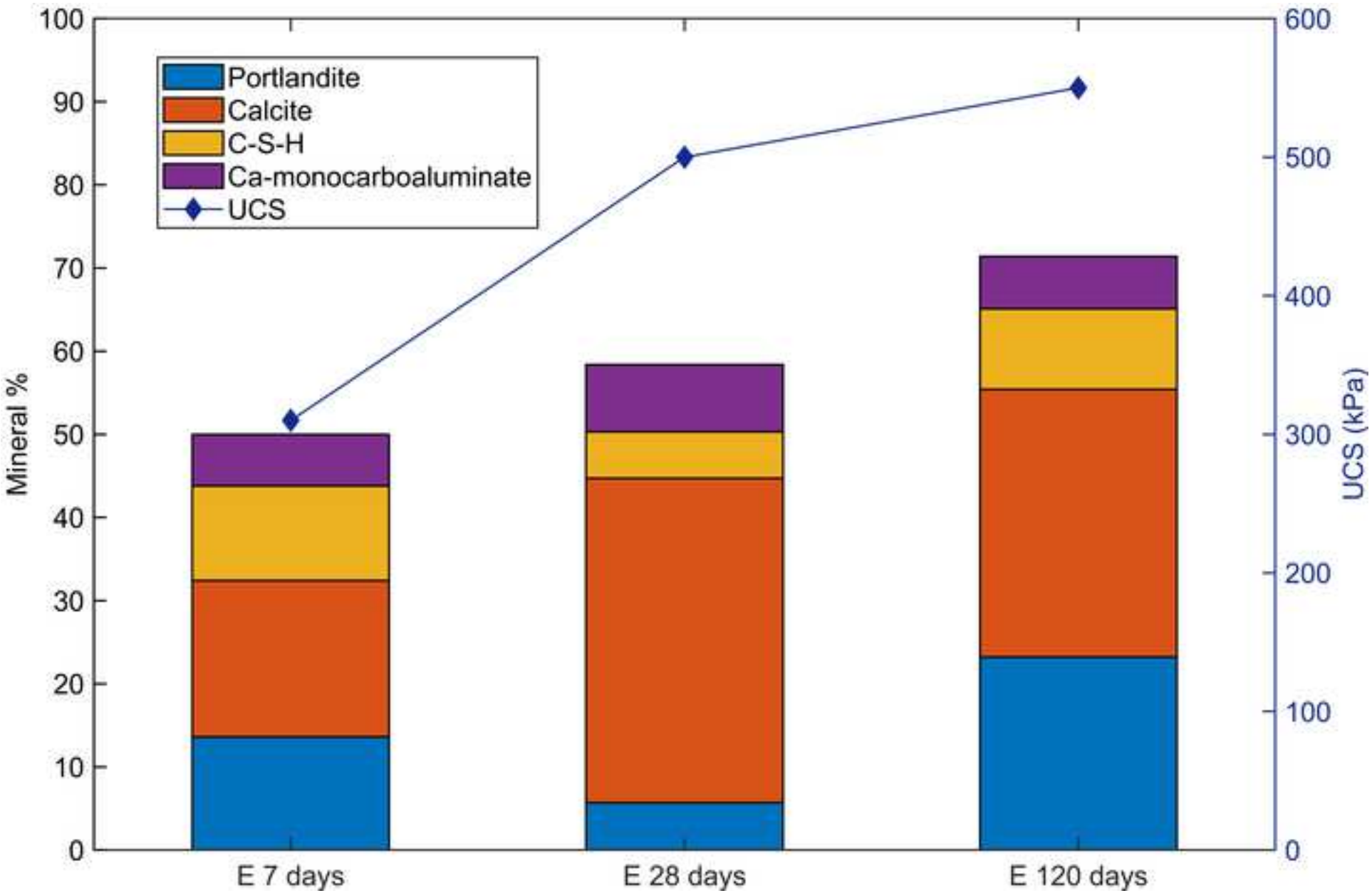

Figure 14

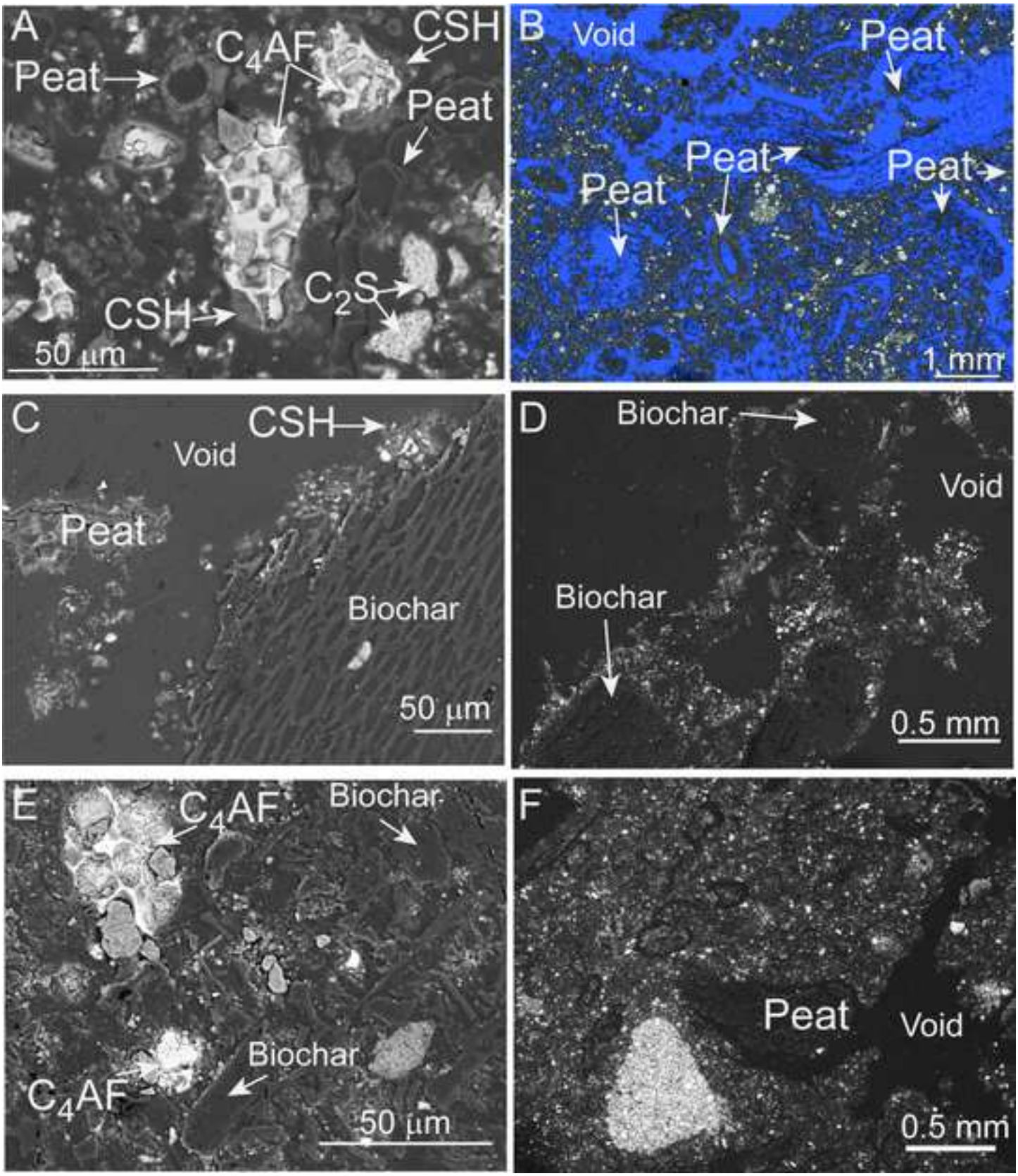

Fig. 1. UCS in OPC-stabilized peat with 5 differently graded biochar filler compared to a sand filler after curing for: A) 7 days; B) 28 days.

Fig. 2. SEM of hydration products in the peat-OPC-biochar mixture. A) SEM image of C-S-H coating and ettringite needles. B) EDS spectra collected at point C33 and area C34.

Fig. 3. Cement hydration on biochar surface. A) SEM of air-dried chip taken from sample C. B) Higher magnification of area marked by white rectangle in A. C) SEM-BSE micrograph of a polished cross section of biochar. Examples of cells and cell walls used for measurements are shown. D) EDS spectrum collected from the point marked A-6 shows composition of Ca, Si and O.

Fig. 4. SEM of peat fragments. A) peat fragment in air-dried chip of a biochar-filler sample. B) peat fragment in air-dried chip of control sample. C) SEM-BSE of control sample, after embedding and polishing. D) SEM-BSE of peat fragment in embedded and polished control sample.

Fig. 5. Microcrystalline calcium carbonate at the edge of biochar. A) SEM-BSE micrograph. B) EDS spectrum from square ROI.

Fig. 6. A) SEM-BSE micrograph of microcrystalline calcium carbonate. B) growth bands are marked by dotted black lines.

Fig. 7. XRD pattern of peat-biochar-OPC, at 7 days of hydration. The position of the most intense reflections of calcite (pdf 00-005-0586), portlandite (pdf 00*044-1481) and C2S (pdf 00-033-0302) are marked.

Fig. 8. Region of the XRD pattern between 22 and 32°2θ. The bottom graphs show the model XRD pattern of two C-S-H phases: dellaite (pdf 04-011-1311) and rosenhahnite (pdf 04-012-8453).

Fig. 9. Two-theta interval of XRD pattern where AFm and Aft peaks occur. The bottom graphs show model peaks of monocarboaluminate (COD 2007668), hemicarboaluminate (COD 2105251), and ettringite (pdf 04-011-5267).

Fig. 10. Rietveld refinement results of sample E XRD. The experimental pattern is shown in black, the curve calculated by Rietveld refinement is in magenta, the gray curve in the bottom graph is the difference between experimental and calculated curves.

Fig. 11. Hydration minerals at seven days. The bar plots show the proportions of hydration minerals in the five samples with biochar filler and in the control. Mineral fractions are normalized to the crystalline portion.

Fig. 12. XRD patterns at 28 days of curing, for samples A and E.

Fig. 13. Progression of OPC hydration and UCS over 120 days, for sample E. Stacked bars show the hydrated mineral fractions at 7, 28 and 120 days. The line plot shows the UCS increase.

Fig. 14. SEM-BSE micrographs of embedded and polished samples show the spatial distribution of peat, OPC and biochar. A) control sample, medium magnification B) control sample, low magnification. C) Sample B, medium magnification. D) Sample B, low magnification. E) Sample E, medium magnification. F) Sample B, low magnification.